Improving the DC-Link Voltage of DFIG Driven Wind System Using Modified Sliding Mode Control

Ravikiran Hiremath* and Tukaram Moger

Department of Electrical and Electronics Engineering, National Institute of Technology Karnataka, Surathkal, Mangalore, India 575025
E-mail: hcravkiran@gmail.com
**Corresponding Author*

Received 01 October 2021; Accepted 10 November 2021;
Publication 27 February 2023

Abstract

The grid-connected doubly fed induction generator (DFIG) driven wind turbine (WT) system encounters voltage fluctuations due to severe grid faults. The rise in DC-link voltage imbalances the system under voltage sag condition. The system's protection should ensure that the WT generator meets the grid requirements through a low voltage ride through (LVRT) technique. This paper proposed the modified 2^{nd} order sliding mode (MSOSM) control with gain added super twisting algorithm (GAST) for LVRT enhancement under voltage sag. This controller adds the low positive gains to the switching functions of the super twisting (ST) algorithm. As a result, it maintains the proper variation margins and constant DC-link voltage of the WT-DFIG system under grid fault. The MSOSM controller suppresses the chattering effect, achieves better zero convergence, and eliminates the coordinate transformations. Moreover, the performance of the proposed controller is compared with existing controllers in the literature with the help of MATLAB/SIMULINK. The hardware-in-loop (HIL) validates these simulation results performed on the OPAL-RT setup. Based on the studies, it is found that the proposed

Distributed Generation & Alternative Energy Journal, Vol. 38_3, 715–742.
doi: 10.13052/dgaej2156-3306.3831

controller enhances the performance of the WT-DFIG system under transient conditions.

Keywords: WT, Gridcodes, DFIG, LVRT, SMC, OPAL-RT, MATLAB.

1 Introduction

Renewable energy sources like solar and wind are gaining much importance over the conventional sources. The more penetration of wind energy significantly raises its industrial sector and market share [1]. Moreover, WT generators are flexible, and offer both fixed speed and variable speed [2]. The DFIG is more preferred in WT generators mainly due to its low losses and less cost over the PMSG during the grid integration. DFIG is one of the variable speed WT generators, where the speed is $\pm 30\%$ around the synchronous speed. Further, rotor side converter (RSC) and grid side converter (GSC) are connected in back-to-back (B2B) form to DFIG system [3]. The main drawback of the DFIG system is sensitivity to faults occurring in it. As a result, it leads to huge generation losses and system would be disconnected. Based on these drawbacks, the literature has suggested the LVRT technique for the DFIG system. Basically, the LVRT keeps the DFIG to remain connected to grid even under the grid faults. The generic control scheme for the WT generators to support LVRT is shown in Figure 1.

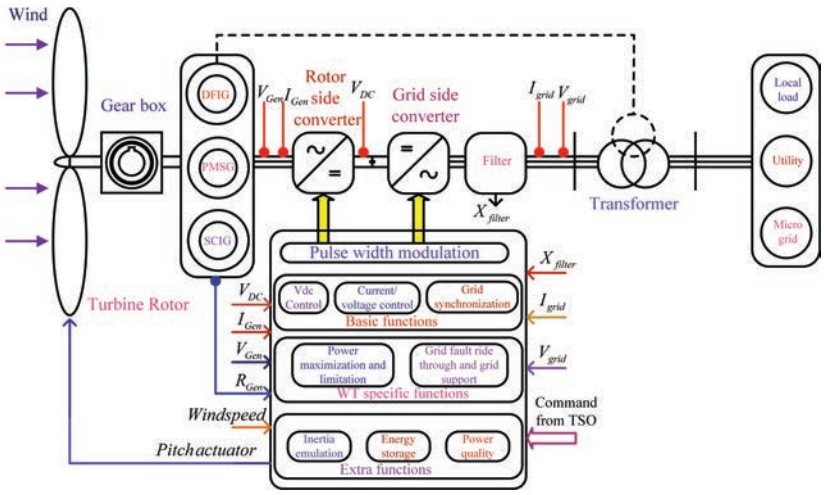

Figure 1 Generic control scheme for the WT generators to support LVRT capabilities.

Table 1 Improved control strategies of DFIG based WT generator system

Author	Controller Strategy	RSC	GSC	Targetted Parameters	Application	Complexity	Remarks
[12]	CFFFB	No	Yes	Vdc, P,Q	WT-Grid	Moderate	Compensation voltage is added to voltage drop at machine terminals
[13]	IARC	Yes	No	P,Q	WF	High	Error compensation term and control variables are considered during design process
[14]	Robust SMC	Yes	No	P,Q	WT-Grid	Simple	Error signals between references and measured rotor currents are presented
[15]	FOSM	Yes	No	Tem	WT-Grid	Simple	Fractional order uncertainity is integrated into control law to compensate parameter uncertainities
[16]	iPISMC	Yes	No	P	WT-Grid	Moderate	Extra input is added to compensate the estimation error
[17]	NERL	Yes	No	P,Q	WT-Grid	Moderate	Boolean control scheme is highlighted

CFFFB-combined feed-forward and feedback, IARC-Improved Adaptive Robust Control, FOSM-fractional order sliding mode control, iPISMC-intelligent proportional-integral sliding mode control, NREL- Novel exponential reaching law

The literature has presented various control strategies for the DFIG system under fault. According to the researchers, the non-linear sliding mode control (SMC) is more preferable for the DFIG system. Further, some of the approaches including higher order and 2^{nd} order SMC (SOSMC) have been developed for the applications such as aerodynamic control [4, 5] and power converters control [6, 7]. In [8], its detailed about the grid fault ride through, where rotor side controller induces the electro-motive force (emf) to DFIG system during fault. An improved rotor side control strategy is developed as rotor power feedback to minimize variations in the voltage of DC link in the WT-DFIG system [9]. The rotor side control improves the internal dynamics and strengthens the DFIG's dynamic behaviour after the fault clearance [10, 11]. In addition, many authors have highlighted the effectiveness of the SMC for WT applications, which is given in the Table 1.

As per the literature, the fault at point of common coupling (PCC) or grid causes more problems, importantly rise in rotor current beyond the rated value, stator current distortion, real and reactive power imbalances, DC-link voltage overshoots to higher nominal value, electromagnetic torque fluctuations, and synchronizing angle variations. The stator side of the DFIG system is more effected as it is directly connected to grid. Further, this undesirable condition violates the grid codes, and consumption of reactive power results in penalty. There are only a few authors, who have addressed these problems and observed less percentage of LVRT enhancement. Therefore, this paper

proposed MSOSM controller (a rotor side controller), emphasizes on some of the problems such as improvement in rotor current, real and reactive power, DC-link voltage, electromagnetic torque, as discussed earlier.

The main focus of the paper is to improve the DC-link voltage in order to stabilize the DFIG system. This improvement in DC-link voltage avoids the reactive power consumption, and tries to maintain the nominal rotor speed and rotor current under the fault condition. The significances of this paper are described as follows:

i. This paper proposes MSOSM controller for improving the LVRT and DC-link voltage of the DFIG system.
ii. This proposed controller is operated with gain added super-twisting (GAST) algorithm.
iii. This paper focuses on improving the DC-link voltage and its other system parameters such as real power, reactive power, rotor current and electromagnetic torque under the voltage sag condition.
iv. The switching controls (S_P and S_Q) are effective with positive gain in them.
v. The analysis of stability and chattering issues strengthen the proposed controller.
vi. This controller regulates the real and reactive power without the flux measurement.
vii. These simulation results are validated with the HIL conducted on the OPAL-RT 4510 setup.

The proposed controller achieves better steady state and transient response when the disturbances arise in the system. Hence, this paper is organized into different sections. In Section 2, modelling of the DFIG based WECS is discussed, Section 3 presents designing of proposed MSOSM controller, Section 4 analyses the stability of the system. In Section 5, simulations and experimental validations are addressed, and then followed by the conclusion.

2 Modelling of DFIG Based Wind Energy Conversion System (WECS)

2.1 WT Modelling

The WT's mechanical power output is set by [11],

$$P_m = \frac{1}{2}\rho C_p(\lambda, \beta) A v^3 \tag{1}$$

Where, P_m = Mechanical power transmitted to the shaft, C_p = Power co-efficient, and it relies on pitch angle of the rotor blades (β) and tip speed ratio (λ),v = Wind velocity(m/s), ρ = Air density (1.225 Kg/m^3), and A = Rotor area (m^2).

The calculated power co-efficient is given by,

$$C_p(\lambda, \beta) = C_1(C_2 - C_3\beta - C_4\beta^2 - C_5)e^{-C_6} \tag{2}$$

Where $C_1 = 0.5$, $C_2 = 116/\lambda_i$, $C_3 = 0.4$, $C_4 = 0$, $C_5 = 5$, $C_6 = 12.5/\lambda_i$, and $\frac{1}{\lambda_i} = \frac{1}{(\lambda+0.08\beta)} - \frac{0.035}{(\beta^3+1)}$

The tip speed ratio is given by,

$$\lambda = \frac{\omega R}{v} \tag{3}$$

Where, ω is rotor rotational speed in rad/sec, *R* is the radius of the rotor blade in m.

2.2 DFIG Modelling

DFIG is one of the variable speed wind generators, whose speed varies by approximately $\pm 30\%$ of the rated speed [18]. DFIG based WECS is shown in Figure 2. DFIG is essentially a wound rotor, where the stator is associated directly while the rotor is linked to the grid with a back-to-back (B2B) converter [19, 20].

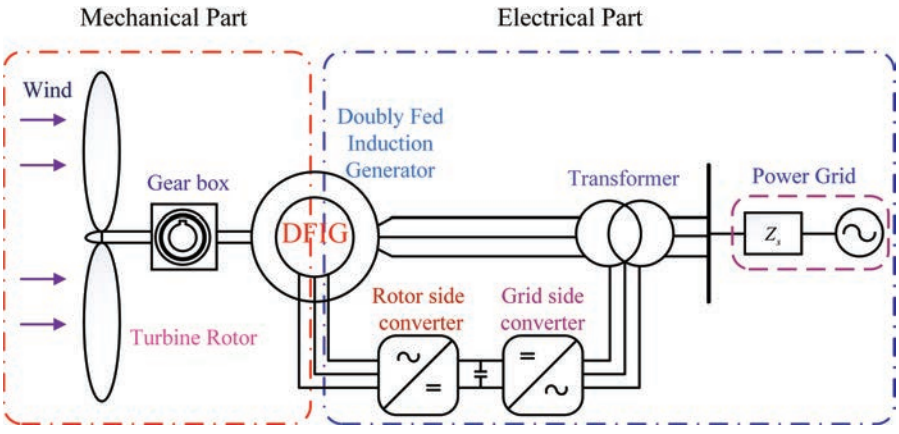

Figure 2 Basic layout of the WT generator with DFIG.

DFIG is modelled using the set of stator and rotor equations. Hence, stator and rotor dynamic voltage equations in a synchronous reference frame are provided by [21, 22]

$$\begin{aligned} U_{ds} &= \frac{d}{dt}(\lambda_{ds}) - \omega_s \lambda_{qs} + R_s I_{ds} \\ U_{qs} &= \frac{d}{dt}(\lambda_{qs}) + \omega_s \lambda_{ds} + R_s I_{qs} \\ V_{dr} &= \frac{d}{dt}(\lambda_{dr}) - (\omega_s - p\omega_r)\lambda_{qr} + R_r I_{dr} \\ V_{qr} &= \frac{d}{dt}(\lambda_{qr}) - (\omega_s - p\omega_r)\lambda_{dr} + R_r I_{qr} \\ P_s &= \frac{3}{2}(U_d I_{ds} + U_q I_{qs}) \\ Q_s &= \frac{3}{2}(U_q I_{ds} - U_d I_{qs}) \end{aligned} \tag{4}$$

where U and V are the constant grid voltage and the voltage controlled, λ stand for flux, p is number of pole pairs, R_s is stator resistance, R_r is rotor resistance, and L_m is mutual inductance.

Besides, the realized standard frame technique for DFIG operation is stator-flux-oriented controller frame. This method consistently recognizes the DFIG's synchronous rotating flux axis [23]. The S-FOC primarily regulates the electrical torque and stator flux independently by orthogonal rotor currents i_{dr} and i_{qr} respectively.

The stator flux control technique is used to align the frame of reference with the d-axis stator flux component, it means $\lambda_{qs} = 0$. Hence, electromagnetic torque reduces to

$$T_e = -\frac{3}{2} p \frac{L_m}{L_s}(\lambda_{ds} I_{qr}) \tag{5}$$

On the other side, C_p value would be maximum at $\lambda = \lambda opt$ for the maximum power extraction. It can be accomplished with optimum rotational speed by the generator, and is given by

$$\omega_{r,opt} = \frac{\lambda_{opt} n_g}{R} v \tag{6}$$

Where n_g is the gear ratio. The rotor side controller therefore adapts the speed of the generator $\omega_r^{ref} = \omega_{r,opt}$

2.3 DFIG Control Strategy

The DFIG control strategy deals with the designing of the SMC, which is based on the Lyapunov application. The basic idea of the SMC technique is to bring the system state vector towards the sliding surface and then the system slides to the desired equilibrium point on that surface. The sliding surface on the sliding motion specifies a system's position or relative degree. Relative degree of the system with grid-connected is controlled by the 1^{st} order SMC (FOSMC) or SOSMC.

To define the sliding surface, the fundamental equation is given by

$$S(X) = \left(\frac{d}{dt} + \lambda\right)^{n-1} e(X) \tag{7}$$

$e = X^* - X$ is the error, *n* is relative degree and λ is a positive co-efficient.

2.3.1 First-Order SMC (FOSMC)

Since the control method is used to identify the active power reference, the first-order sliding surfaces reflect the error between the measured powers and their references can be expressed as follows [15].

$$S_{dq} = \begin{bmatrix} S_d(Q_s) \\ S_q(P_s) \end{bmatrix} = \begin{bmatrix} e(Q_s) \\ e(P_s) \end{bmatrix} \tag{8}$$

Where $e(Qs) = Q_s^* - Q_s$ and $e(Ps) = P_s^* - P_s$. Then, their derivatives are:

$$\dot{S}_{dq} = \begin{bmatrix} \dot{S}_d(Q_s) \\ \dot{S}_q(P_s) \end{bmatrix} = \begin{bmatrix} \dot{Q}_s^* - \dot{Q}_s \\ \dot{P}_s^* - \dot{P}_s \end{bmatrix} \tag{9}$$

The chattering effect is the disadvantage of this SMC. However, lyapunov theory is used in this sliding mode control, which verifies the zero-convergence of sliding surfaces and also improves the stability. Thus, the following condition is satisfied [8]

$$\dot{V} = S^T \dot{S} < 0 \tag{10}$$

2.3.2 Second-Order SMC (SOSMC)

The second order slides around the boundaries are defined as follows:

$$S_{dq} = \begin{bmatrix} S_d(Q_s) \\ S_q(P_s) \end{bmatrix} = \begin{bmatrix} e(Q_s) + b_Q \int e(Q_s) \\ e(P_s) + b_P \int e(P_s) \end{bmatrix} \tag{11}$$

The discontinuous function is replaced by a smooth approximation to overcome the chattering effect. The higher-order is a good alternative for

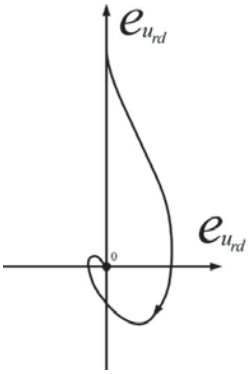

Figure 3 Super-twisting algorithm phase trajectory.

reducing the chattering effect [16]. The main problem in the higher order is requirement of the more information. Notably, the application of an n^{th} order controller involves the knowledge of $\dot{S}$, $\ddot{S}$, $\ldots S^{n-1}$. To overcome this problem, the super-twisting algorithm is used, which requires only sliding surface information and is shown in Figure 3.

3 Designing of Proposed MSOSM Controller

The switching controls for RSC interms of stator real and reactive power are chosen for improving the dynamic response and is given by

$$S_P = (P_s^* - P_s) + c_P \int (P_s^* - P_s)dt + G_1 \tag{12}$$

$$S_Q = (Q_s^* - Q_s) + c_Q \int (Q_s^* - Q_s)dt + G_2 \tag{13}$$

Where, c_P and c_Q are added to eliminate steady state errors, G_1 and G_2 are the gains to smoothening the variations, P_s^* is stator real power reference and Q_s^* is the reference value of stator reactive power.

The time derivatives of the S_P and S_Q are given by:

$$\begin{aligned}\dot{S}_P = {} & \frac{L_m}{\sigma L_s L_r} u_s \left[(R_r - c_P \sigma L_r) i_{rd} - \sigma \omega_{s1} L_r i_{rq} + \omega_{s1} \frac{L_m}{L_s} \lambda_s \right] \\ & + P_s^* + c_P P_s^* - \frac{L_m}{\sigma L_s L_r} u_s u_{rd}\end{aligned} \tag{14}$$

$$\begin{aligned}\dot{S}_Q = \frac{L_m}{\sigma L_s L_r} u_s \left[(-R_r - c_Q \sigma L_r) i_{rq} - \sigma \omega_{s1} L_r i_{rd} - c_Q \frac{\sigma L_r}{L_m} \lambda_s\right] \\ + Q_s^* + c_Q Q_s^* + \frac{L_m}{\sigma L_s L_r} u_s u_{rq}\end{aligned} \tag{15}$$

The RSC voltages regulate the stator real and reactive power of the DFIG and is given by

$$\begin{aligned}\frac{\partial \dot{S_P}}{\partial u_{rd}} = \frac{-L_m u_s}{\sigma L_s L_r} \neq 0 \\ \frac{\partial \dot{S_Q}}{\partial u_{rq}} = \frac{L_m u_s}{\sigma L_s L_r} \neq 0\end{aligned} \tag{16}$$

However, as per the literature, the non-linear 2^{nd} order and higher-order SMC suppress the chattering effect and enhances the controlling effect precisely [15]. Here, if the partial derivatives of S_P and S_Q are equal to zero, then equivalent control terms in Equation (17) would be zero. Then, it leads to poor controller performance. Further, the control laws are applied on the rotor side voltages, which is given by,

$$\begin{aligned}u_{rd} = \Delta u_{rd} + u_{rdeq} \\ u_{rq} = \Delta u_{rq} + u_{rqeq}\end{aligned} \tag{17}$$

where, $\Delta u_{rd}, \Delta u_{rq}$ are control terms and u_{rdeq}, u_{rqeq} are equivalent control terms by letting $\dot{S_P}, \dot{S_Q} = 0$.

The Equation (17) [19], composed of switching control terms, which converges the sliding surface to zero in finite time with the help of gain added super-twisting (GAST) algorithm. In addition, this algorithm speed up the system transient response and reduces the steady-state errors. According to the Lyapunov application [17], the rotor side voltages as per the GAST algorithm are given by

$$\begin{aligned}\Delta u_{rd} = K_{p1} \sqrt{\mid S_P \mid} sgn(S_P) + K_{p2} \int sgn(S_P) dt + G_1 S_Q \\ u_{rdeq} = \frac{\sigma L_s L_r}{L_m u_s} [P_s^* + c_P (P_s^* - P_s)] + R_r i_{rd} - \sigma \omega_{sl} L_r i_{rq} \\ + \frac{\omega_{sl} L_m}{L_s} \lambda_s\end{aligned} \tag{18}$$

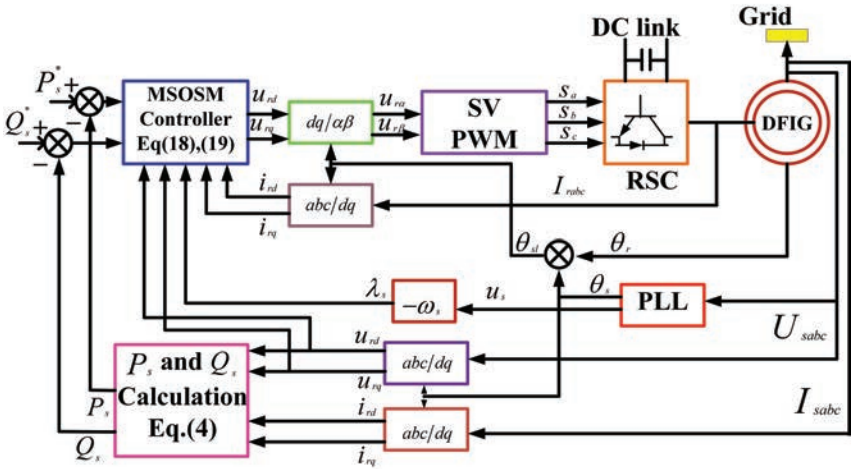

Figure 4 Proposed controller of MSOSMC diagram.

$$\Delta u_{rq} = -K_{q1}\sqrt{|\ S_Q\ |}sgn(S_Q) - K_{q2}\int sgn(S_Q)dt - G_2 S_P$$
$$u_{rqeq} = \frac{\sigma L_s L_r}{L_m u_s}[Q_s^* + c_Q(Q_s^* - Q_s)] + R_r i_{rq} - \sigma\omega_{sl} L_r i_{rd} \tag{19}$$

where, K_{p1}, K_{q1}=0.1, K_{p2}, K_{q2}=3, and G_1, G_2=2 are tuned positive constants. The equivalent control terms are obtained after solving the Equations (14) and (15). Besides, the rotor side control strategy, which is applied for DFIG system is depicted in Figure 4.

3.1 Chattering of the Proposed MSOSM Controller

The chattering effect in the SMC is unavoidable. This effect is mainly due to high frequency switching control action and can be mitigated by the higher order SMC methods. Some of the authors have compared the chattering amplitudes of various conventional SMC. Based on this comparison, it is found that chattering problem delays the finite time convergence (FTC) s = 0 of a system.

The chattering problem is a presence of unmodelled dynamics with discontinuous control. These dynamics of a system is given by the transfer function (TF) $\frac{1}{(\mu s+1)^2}$. This transfer function is modelled with the plant in order to suppress the chattering effect. The block diagram of plants with chattering effect shown in Figure 5 are of conventional ST algorithm and

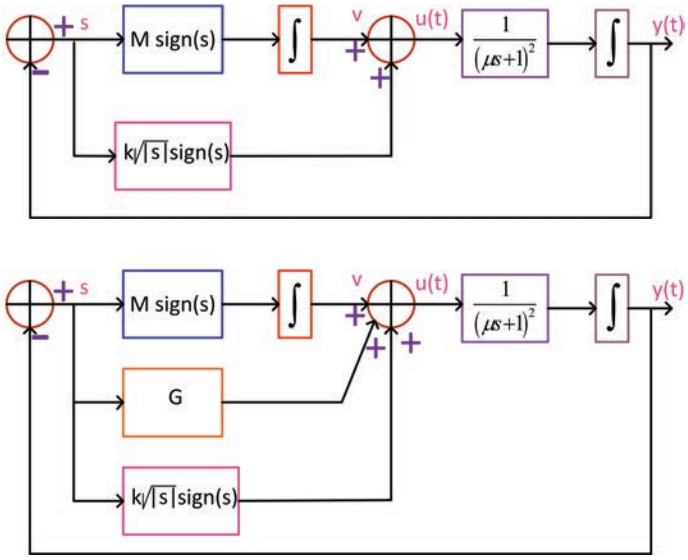

Figure 5 Block diagram of plants with chattering problem (a) ST algorithm (b) GAST algorithm.

Table 2 Comparison of the proposed controller with conventional SMC

	1^{st} Order Controller	ST Controller	Proposed Controller
Amplitude of the output chattering	4.81×10^{-4}	1.27×10^{-4}	1.24×10^{-6}

GAST algorithm respectively. Here, the block diagram included the 2^{nd} order TF as a chattering effect, and sign(s) indicates the signum fuction of sliding surface. Amplitudes of the chattering is given in Table 2 to highlight the advantage of GAST algorithm in the proposed MSOSM controller. The outputs of these plants are shown in Figure 6, and observed more variations in ST algorithm compared to GAST algorithm. Based on these outputs, it is found that GAST algorithm in the proposed controller is more effective than ST algorithm in the conventional SM controllers.

4 Stability Analysis

The stability analysis is done for the DC-link voltage of a DFIG system under the sag condition. The dynamics of the DC-voltage interms of 2^{nd} order

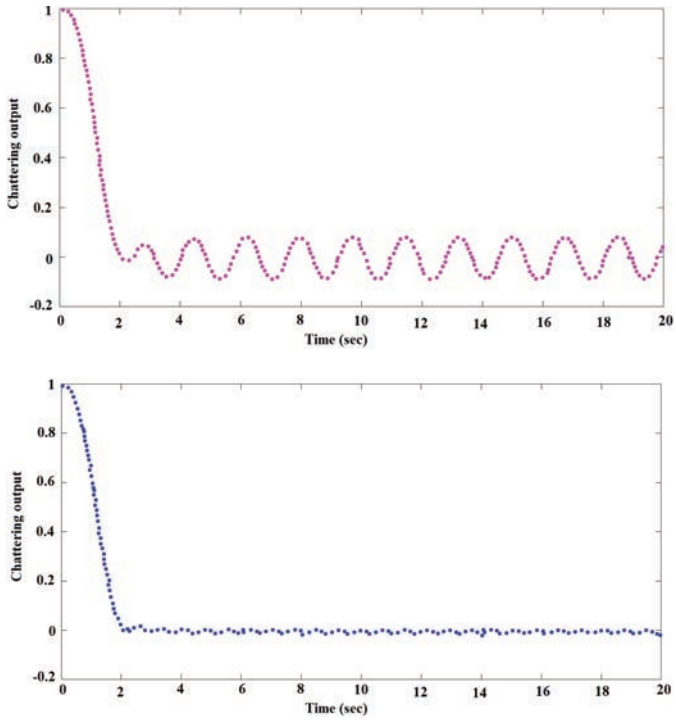

Figure 6 Chattering output of the plants (a) ST algorithm (b) GAST algorithm.

transfer function is extracted, and is given by

$$\frac{\Delta V_{dc}}{\Delta P_{conv}} = \frac{S/CV_{dc}}{S^2 + \frac{1.5k_v}{C}(k_G + k_P) + \frac{1.5k_v k_I}{C}} \tag{20}$$

where, ΔV_{dc} is Disturbance in the DC-link voltage, $k_v = \frac{V_g}{V_{dc}}$, V_g is grid side voltage (V), $k_G = \frac{i_g}{V_{dc}}$, i_g is grid side current (A), and ΔP_{conv} is rotor side quantity.

The Equation (20) is used for obtaining the bode plots and step responses with varying damping ratios as shown in Figure 7. The increasing in damping ratios indicate the reduction of peak DC ripples, later it results in reduction of current overshoot. Importantly, the main function of DC-link control is only to smoothing.

In the Figure 7, damping ratios are varied from 0.1 to 2.5 in order to inspect the disturbance rejection and settling time period. The bode plots

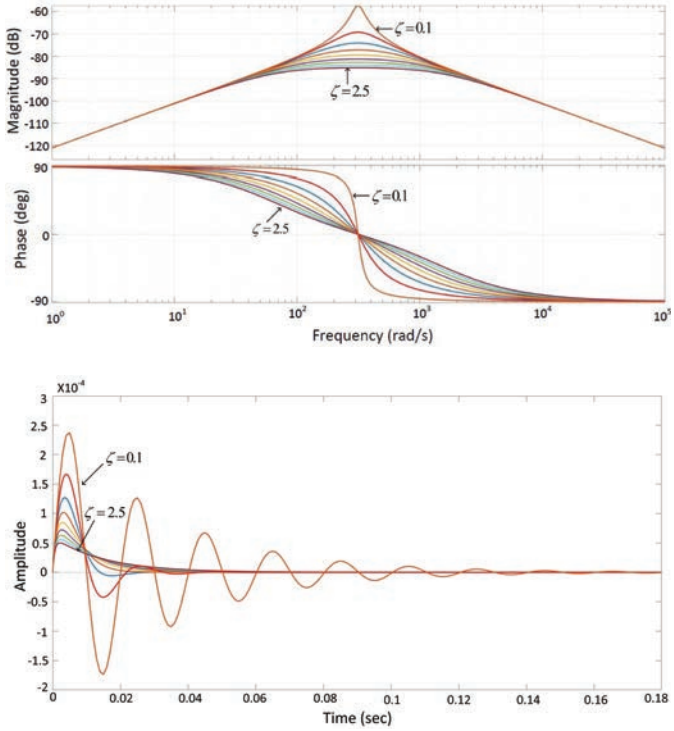

Figure 7 Bode plots and step responses for various damping ratios under disturbance (a) bode plot (b) step response.

switch from instability to stable loops as it moves from 0.1 to 2.5. But, the settling time period of the step response increases as the damping ratios progress in ascending order. Also, the significant smoothing can be observed in it.

5 Simulations and Experimental Validations

This section evaluates the performance of proposed MSOSM controller using the MATLAB/Simulink software and validated with OPAL-RT 4510 setup, as shown in Figure 8. The parameters employed in the simulation are listed in Table 3. The schematic control strategy for the proposed MSOSM controller is shown in Figure 4.

The hardware setup for the simulation model is done through OPAL-RT 4510. The OPAL-RT is a hardware-in-loop (HIL) and its specifications are given in Table 4. The simulink model is built in this OPAL-RT by creating

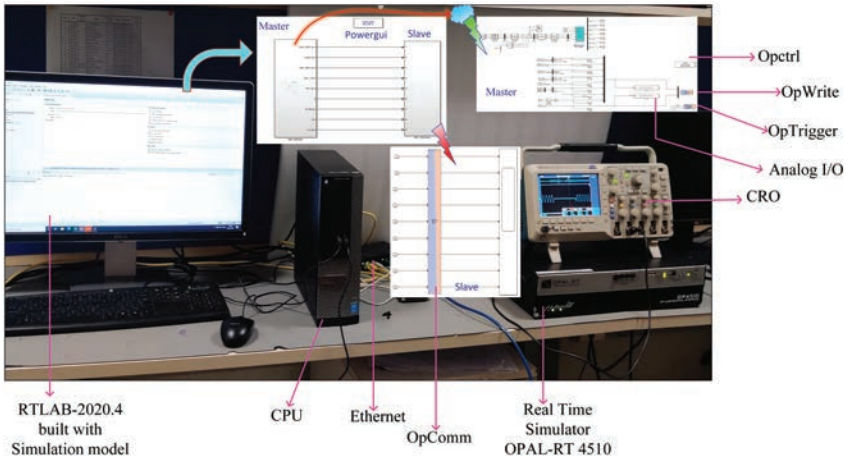

Figure 8 Hardware-in-loop setup in OPAL-RT 4510 simulator.

Table 3 1.5MW DFIG based WT parameters

Symbol	Value
R_s	0.023 pu
R_r	0.016 pu
L_s	0.18 pu
L_r	0.16 pu
L_m	2.9 pu
C	1.15 pu
p	3
R	35 m
b	0.00015 N*m*sec/rad
J	765.6 kg*m^2
n_g	62.5
β	0^0
ρ	1.2 kg/m^3
λ_{opt}	6.325
ω_s	2π50 rad/sec
$\sqrt{u_{ds}^2 + u_{qs}^2}$	575 V (rms)

the master and slave subsystem as shown in Figure 8. In addition, the master subsystem includes hardware interfaces, such as OpWrite and OpTrigger block which helps to store model data, OpCtrl block which provides the binstream files for the simulator to execute the model, and Analog I/O block which helps to record the waveforms in CRO. Further, in the slave subsystem,

Table 4 Specifications of OPAL-RT 4510 simulator

1	Real time Simulation Software	RT-LAB
2	Real time operating system	Linux REDHAT
3	FPGA	Xilinx KINTEX-7
4	Sampling time	200MHz
5	CPU	Intel Xeon E3 4-core 3.5 GHz
6	Connectivity	Ethernet RS-232
7	High-speed optical interface	4 SFP sockets, up to 5Gbps
8	Analog I/O systems	16 channels
9	Digital I/O systems	32 channels

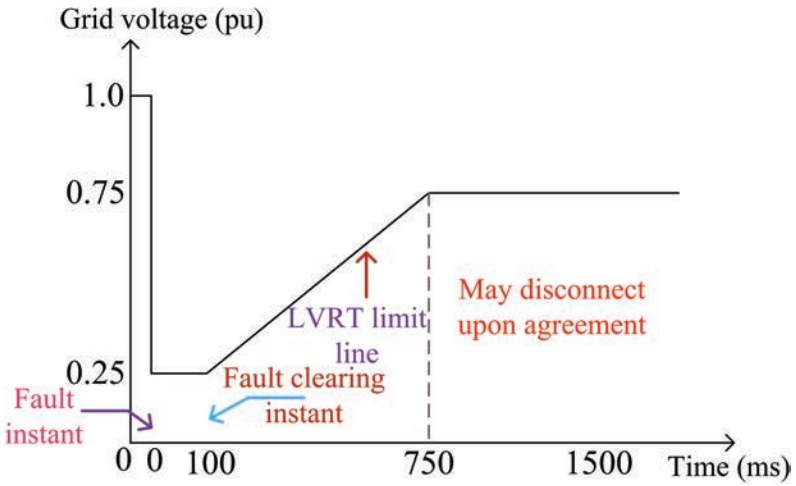

Figure 9 Danish grid code.

the OpComm block is used to verify the offline simulation results prior to the interfacing with simulator, later model is built in RTLAB-2020.4 software, and model is loaded to the simulator for validating the simulation results.

The voltage sag is created as a fault at PCC. The 60% of the voltage sag is active for the duration of 100 ms and after that the fault has been cleared. This proposed DFIG based WECS model follows the Danish grid code specifications as shown in Figure 9 [24]. According to this grid code, the system under fault for 100 ms has to recover 75% of the nominal grid voltage within 750 ms, otherwise system to be disconnected from the grid.

5.1 Control Performance Under No Fault/Disturbance

The performance evaluation of the DFIG based WT generator is carried out using the MSOSM controller and is shown in Figure 11. This proposed controller enables the DFIG system for maintaining the constant DC-link voltage of 1.15 pu between the RSC and GSC. As a result, the 1.5 MW of constant power is transferred to the grid without the consumption of reactive power. The rotor current is undistorted and also helps in providing the constant power. The electromagnetic torque is constant without affecting the rotor speed of the DFIG. The hardware validation for these simulation results of the proposed controller is not shown as it is under no fault condition.

5.2 Control Performance During Voltage Sag

The control performance of the proposed controller during voltage sag is shown in Figure 11 and the hardware-in-loop setup is shown in Figure 8. Here, the hardware validation is shown for the proposed controller under the voltage sag condition.

This sag is created for 100 ms, which is initiated at t = 0.3 s and cleared at t = 0.4 s. Thereby, the DC-link voltage fluctuated from 1.25 pu to 1.2 pu during fault initiation and clearance. The hardware results can be seen in Figure 11, and are approximated to the simulation results as shown in Figure 12. The amplitude of this capacitor voltage comes down due to GAST algorithm. This GAST based MSOSM targetted the DC-link voltage in order to balance the system during sag. As a result, the rotor current distorts and reaches up to 1.85 pu during the fault period, but the rotor current in the hardware result is 1.2 pu as it is due to interfacing effect and changes in the initial condition settings in the model. Later it takes fraction of seconds to recover and settle. The fluctuations of active power is from 0.5 pu to 2.5 pu during the sag period, but in the hardware, it is showing approximated result. Then, the reactive power varies from 0.6 pu to -1.1 pu and same variations can be seen in hardware results. The sag effect fluctuates the voltage even after the fault clearance. Moreover, the electromagnetic torque rises from -0.1 pu to -2.5 pu during the instant of fault and clearance of fault respectively.

The DFIG system under the fault has been discussed in three cases by comparing the 1^{st} order SMC, 2^{nd} order SMC, and proposed controller. These cases are studied as follows:

Case A: Effect of 1^{st} order SMC on DFIG system

The system under this controller is ineffective due to inefficient operation of switching functions during fault. Also, the chattering effect is the common

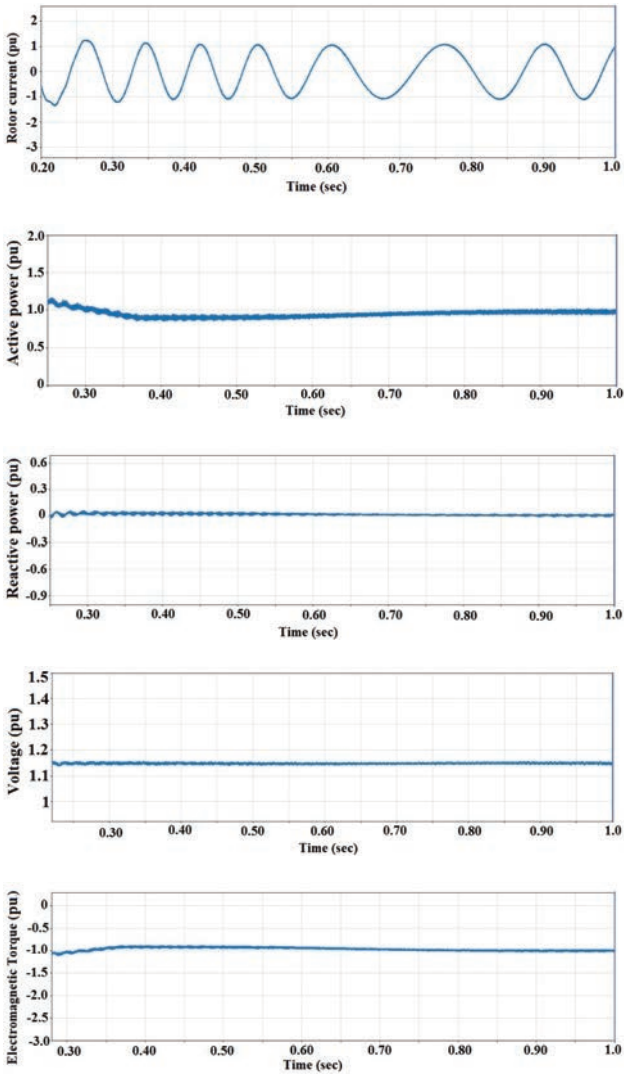

Figure 10 LVRT capability of DFIG without grid fault with the proposed controller (a) rotor current (b) active power (c) reactive power (d) DC-link voltage (e) electromagnetic torque.

problem in 1^{st} order SMC. In view of these problems, the DFIG system under fault is unable to enhance the LVRT technique. The system parameters especially DC-link voltage is below the rated value with large chattering and never settled after the fault clearance. The simulation results of this controller can be observed in the Figure 13.

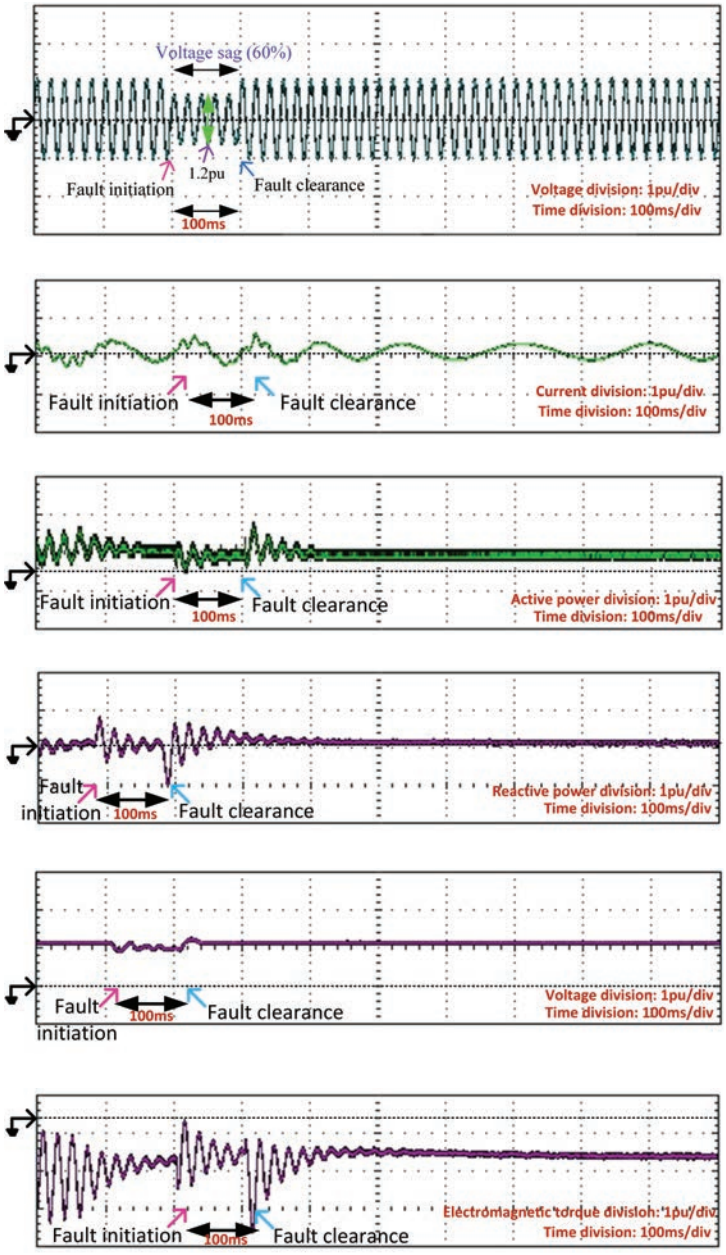

Figure 11 Hardware results of LVRT capability of DFIG with the proposed controller under 60% voltage sag (i) stator voltage (ii) rotor current (iii) active power (iv) reactive power (v) DC-link voltage (vi) electromagnetic torque.

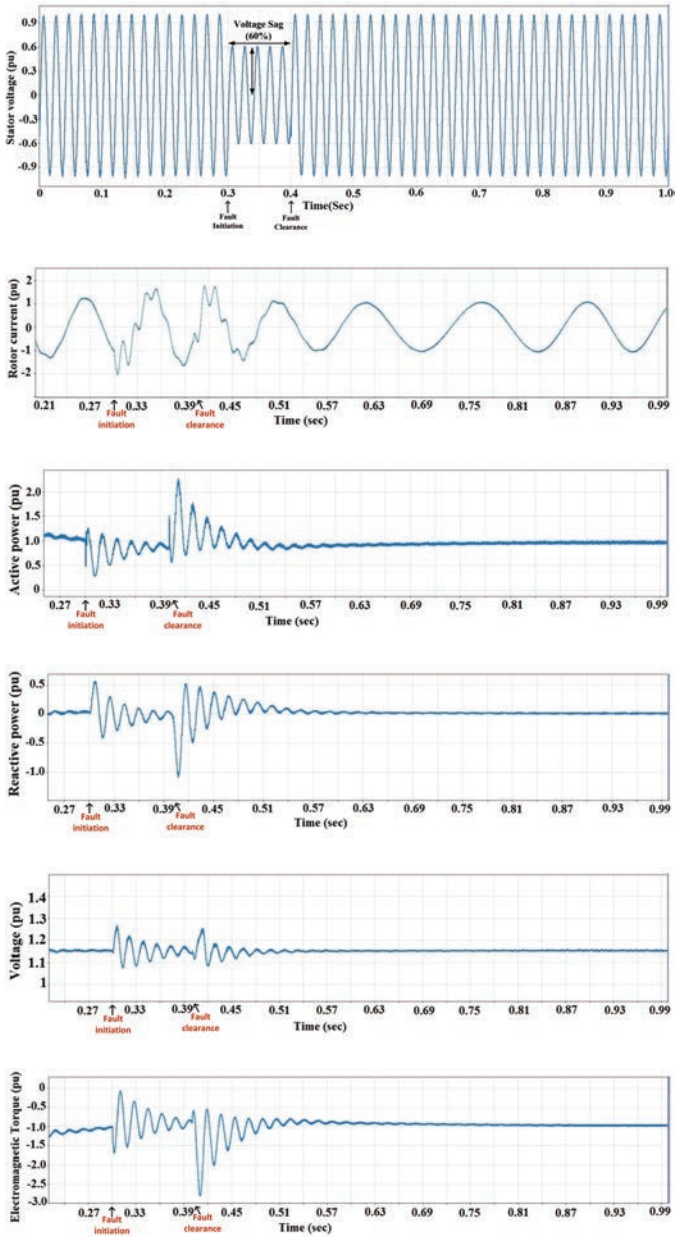

Figure 12 Simulation results of LVRT capability of DFIG with the proposed controller under 60% voltage sag (1) stator voltage (2) rotor current (3) active power (4) reactive power (5) DC-link voltage (6) electromagnetic torque.

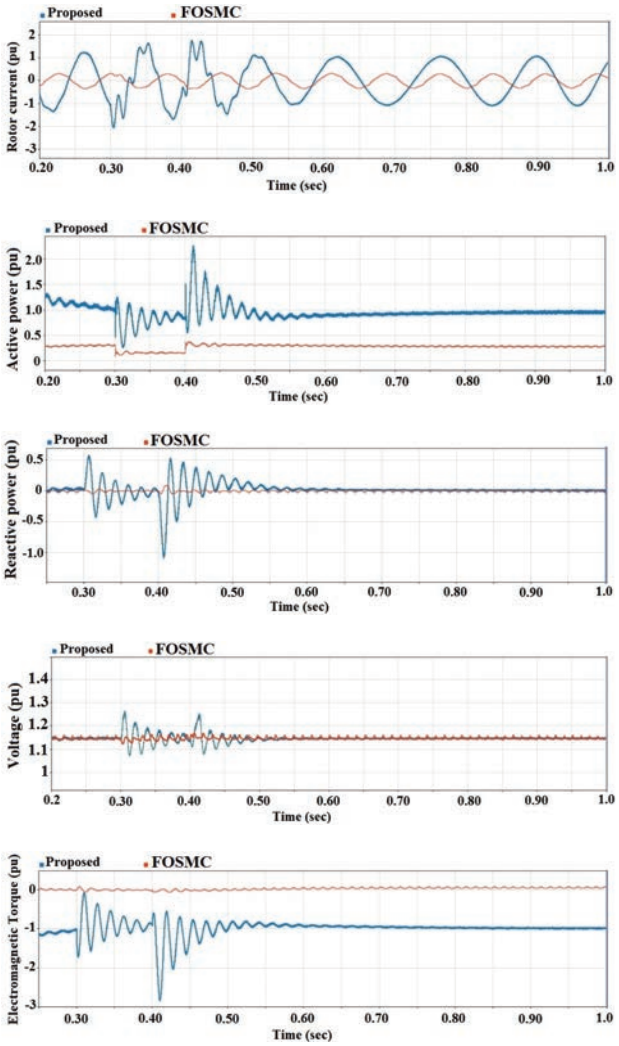

Figure 13 Comparison of FOSMC and proposed controller during LVRT mechanism of DFIG system during grid fault (a) rotor current (b) active power (c) reactive power (d) DC-link voltage (e) electromagnetic torque.

Case B: Impact of 2^{nd} order SMC on DFIG based WT generator

The switching functions are efficient and super-twisting algorithm is used in SOSM. But, the peak amplitudes of the system parameters, importantly DC-link voltage is a concern on the stability of the system. Also, some amount of chattering is a problem. The simulation results compared with the proposed

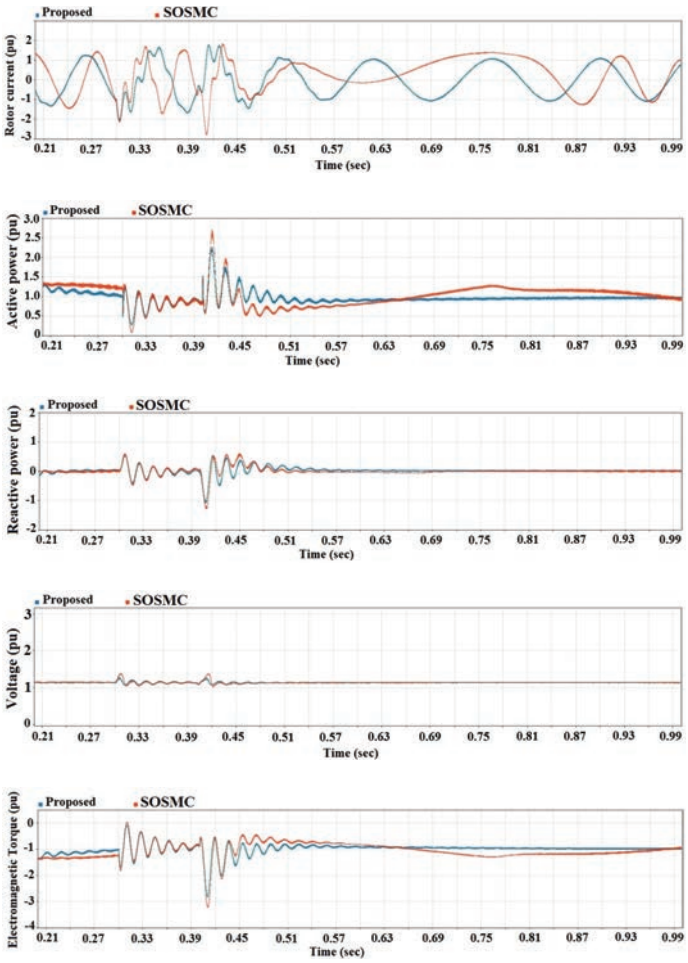

Figure 14 Comparison of SOSMC and proposed controller during LVRT mechanism of DFIG system during grid fault (a) rotor current (b) active power (c) reactive power (d) DC-link voltage (e) electromagnetic torque.

controller under sag can be seen in the Figure 14. However, 2^{nd} order SMC is better compared to 1^{st} order SMC.

Case C: Performance of the proposed controller on DFIG system

The modification in the switching functions and GAST algorithm of the MSOSM resulted in large improvement in the behaviour of DFIG system under fault condition. This proposed controller enhances the LVRT by reducing the peak values of the DC-link voltage and other system parameters and

Table 5 Comparison of the proposed controller with 1^{st} order SMC [15]

Parameters	1^{st} Order SMC	Proposed
Rotor current	0.2 pu	1.7 pu
Stator real power	0.15 pu	1 pu
Stator reactive power	0 pu	−0.4 pu
DC link voltage	1.12 pu	1.25 pu
Electromagnetic torque	0 pu	−1.7 pu

Table 6 Comparison of the proposed controller with 2^{nd} order SMC [16]

Parameters	2^{nd} Order SMC	Proposed
Rotor current	1.6 pu	1.2 pu
Stator real power	0.05 pu	0.35 pu
Stator reactive power	−0.5 pu	−0.35 pu
DC link voltage	1.18 pu	1.12 pu
Electromagnetic torque	−1.8 pu	−1.6 pu

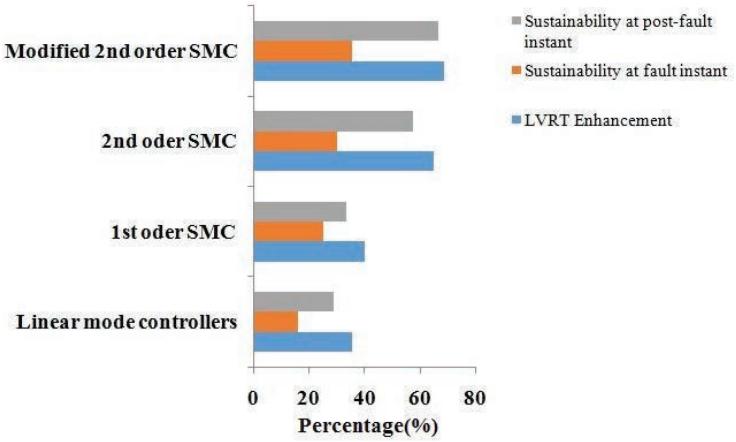

Figure 15 Comparative study of efficient controllers.

validated by the HIL as shown in Figure 11. The comparison is done with the existing controllers in the literature. This comparison is also tabulated in Tables 5 and 6. The system parameters values given in these tables reveal the attained peak values during the grid fault. The comparisons clearly show the merits of the proposed controller as it makes the system convergence better. In addition, the comparison chart between the controllers are made, as seen in Figure 15.

6 Conclusion

This paper proposed the MSOSM controller for grid-connected DFIG system. The perspective of the LVRT enhancement is analysed through this proposed controller under the voltage sag condition, and the conclusions are drawn as follows:

i. The hardware in loop (OPAL-RT 4510) results are closely matched with the simulation results, which is validation to the proposed controller under the voltage sag.
ii. The model's hardware RT-LAB interface and initial condition settings are mainly responsible for the approximate matching from the exact matching, while comparing the results.
iii. The Lyapunov analysis brought the modification in the proposed controller and improved the system's performance.
iv. The analysis of stability and chattering problems indicated the effectiveness of the proposed controller.
v. The GAST algorithm based proposed controller improved the transient behaviour of the machine parameters, such as DC-link voltage, real power, reactive power, rotor current, and electromagnetic torque under the voltage sag.
vi. The proposed controller suppressed the uncertainties and its minimal discontinuous component as it overcame the chattering problem and peak amplitude.
vii. This paper simplified the controller design by choosing the SMC approach over the coordinate transformations.
viii. The MSOSM controller provided better results as compared to 1^{st} order SMC, and 2^{nd} order SMC.
ix. Based on the results, it is found that LVRT enhancement is achieved with the improved transient performance.

References

[1] Liang Wang, Xiaorong Xie, Qirong Jiang, Hui Liu, Yu Li, and Huakun Liu. Investigation of ssr in practical dfig-based wind farms connected to a series-compensated power system. *IEEE Transactions on Power Systems*, 30(5):2772–2779, 2014.

[2] Chia-Tse Lee, Che-Wei Hsu, and Po-Tai Cheng. A low-voltage ride-through technique for grid-connected converters of distributed energy

resources. *IEEE Transactions on Industry Applications*, 47(4):1821–1832, 2011.

[3] M Tarafdar Hagh, Kashem M Muttaqi, Danny Sutanto, MSA Hossain, and Ahmed MA Haidar. Improving fault ride-through capability of dfig based wind generators by using bridge-type superconducting fault current limiter. In *Power Engineering Conference (UPEC), 2015 50th International Universities*, pages 1–6. IEEE, 2015.

[4] Mohammad Javad Morshed and Afef Fekih. A comparison study between two sliding mode based controls for voltage sag mitigation in grid connected wind turbines. In *2015 IEEE Conference on Control Applications (CCA)*, pages 1913–1918. IEEE, 2015.

[5] Brice Beltran, Tarek Ahmed-Ali, and Mohamed El Hachemi Benbouzid. High-order sliding-mode control of variable-speed wind turbines. *IEEE Transactions on Industrial electronics*, 56(9):3314–3321, 2008.

[6] Shuying Yang, Tianbao Zhou, Dengyue Sun, Zhen Xie, and Xing Zhang. A scr crowbar commutated with power converter for dfig-based wind turbines. *International Journal of Electrical Power & Energy Systems*, 81:87–103, 2016.

[7] Vijay Chand Ganti, Bhim Singh, Shiv Kumar Aggarwal, and Tara Chandra Kandpal. Dfig-based wind power conversion with grid power leveling for reduced gusts. *IEEE Transactions on Sustainable Energy*, 3(1):12–20, 2011.

[8] Yuan-Kang Wu and Wu-Han Yang. Different control strategies on the rotor side converter in dfig-based wind turbines. *Energy Procedia*, 100:551–555, 2016.

[9] Jiabing Hu, Yunhui Huang, Dong Wang, Hao Yuan, and Xiaoming Yuan. Modeling of grid-connected dfig-based wind turbines for dc-link voltage stability analysis. *IEEE Transactions on Sustainable Energy*, 6(4): 1325–1336, 2015.

[10] Muhammad Arif Sharafat Ali, Khawaja Khalid Mehmood, Shazia Baloch, and Chul-Hwan Kim. Modified rotor-side converter control design for improving the lvrt capability of a dfig-based wecs. *Electric Power Systems Research*, 186:106403, 2020.

[11] Ravikiran Hiremath and Tukaram Moger. Comprehensive review on low voltage ride through capability of wind turbine generators. *International Transactions on Electrical Energy Systems*, page e12524, 2020.

[12] Rini Ann Jerin Amalorpavaraj, Palanisamy Kaliannan, Sanjeevikumar Padmanaban, Umashankar Subramaniam, and Vigna K Ramachandaramurthy. Improved fault ride through capability in dfig based wind

turbines using dynamic voltage restorer with combined feed-forward and feed-back control. *IEEE Access*, 5:20494–20503, 2017.

[13] Haiying Dong, Ningning Chen, Xiaoqing Li, and Hongwei Li. Improved adaptive robust control for low voltage ride-through of front-end speed regulation wind turbine. *IEEE Access*, 8:55438–55446, 2020.

[14] Mohammed Fdaili, Ahmed Essadki, and Tamou Nasser. Comparative analysis between robust smc & conventional pi controllers used in wecs based on dfig. *International Journal of Renewable Energy Research (IJRER)*, 7(4):2151–2161, 2017.

[15] Sadegh Ebrahimkhani. Robust fractional order sliding mode control of doubly-fed induction generator (dfig)-based wind turbines. *ISA transactions*, 63:343–354, 2016.

[16] Shanzhi Li, Haoping Wang, Yang Tian, Abdel Aitouch, and John Klein. Direct power control of dfig wind turbine systems based on an intelligent proportional-integral sliding mode control. *ISA transactions*, 64: 431–439, 2016.

[17] Yifang Liu, Zhijie Wang, Linyun Xiong, Jie Wang, Xiuchen Jiang, Gehao Bai, Renfu Li, and Sanming Liu. Dfig wind turbine sliding mode control with exponential reaching law under variable wind speed. *International Journal of Electrical Power & Energy Systems*, 96:253–260, 2018.

[18] Abdul Motin Howlader and Tomonobu Senjyu. A comprehensive review of low voltage ride through capability strategies for the wind energy conversion systems. *Renewable and Sustainable Energy Reviews*, 56: 643–658, 2016.

[19] Naggar H Saad, Ahmed A Sattar, and Abd El-Aziz M Mansour. Low voltage ride through of doubly-fed induction generator connected to the grid using sliding mode control strategy. *Renewable Energy*, 80: 583–594, 2015.

[20] David Atkinson, Graham Pannell, Wenping Cao, Bashar Zahawi, Tusitha Abeyasekera, and Milutin Jovanovic. A doubly-fed induction generator test facility for grid fault ride-through analysis. *IEEE Instrumentation & Measurement Magazine*, 15(6), 2012.

[21] Paul C Krause, Oleg Wasynczuk, Scott D Sudhoff, and Steven Pekarek. *Analysis of electric machinery and drive systems*, volume 2. Wiley Online Library, 2002.

[22] Ravikiran Hiremath and Tukaram Moger. Lvrt enhancement of dfig-driven wind system using feed-forward neuro-sliding mode control. *Open Engineering*, 11(1):1000–1014, 2021.

[23] Lihui Yang, Zhao Xu, Jacob Ostergaard, Zhao Yang Dong, and Kit Po Wong. Advanced control strategy of dfig wind turbines for power system fault ride through. *IEEE Transactions on power systems*, 27(2):713–722, 2012.

[24] EMG Rodrigues, GJ Osório, R Godina, AW Bizuayehu, JM Lujano-Rojas, and JPS Catalão. Grid code reinforcements for deeper renewable generation in insular energy systems. *Renewable and Sustainable Energy Reviews*, 53:163–177, 2016.

Biographies

Ravikiran Hiremath received the B.E. degree in electrical and electronics engineering and M.Tech. degree in power electronics from Visvesvaraya Technological University (VTU), Belgaum, Karnataka, India, in 2014 and 2017, respectively. He recently received his Ph.D. degree in Electrical and Electronics Engineering from National Institute of Technology Karnataka (NITK), Surathkal, Mangaluru, India, in 2022. His research interests include grid integration of renewable energy, low voltage ride through capabilities of DFIGs, and converters controllers.

Tukaram Moger received B.E. degree in electrical and electronics engineering from Karnatak University, Dharwad, Karnataka, India, in 2001, M.Tech. degree in electrical engineering from Indian Institute of Technology Kanpur (IITK), UP, India, in 2005, and Ph.D. degree in electrical engineering from Indian Institute of Science (IISc) Bengaluru, India, in 2016. He has been associated with academic institutions as a faculty member and currently working as assistant professor in the Department of Electrical and Electronics Engineering, National Institute of Technology Karnataka (NITK), Surathkal, Mangaluru, India. His research interests include grid Integration of renewable energy, probabilistic approach to power systems, solar photovoltaic systems, wind energy conversion systems, power system operation and planning, reactive power and voltage control, machine learning applications to power systems. He is a senior member of IEEE (USA), IEEE Power & Energy Society (PES), member of IEEE Eta-Kappa Nu (Mu Xi Chapter of IISc), IET (UK), CIGRE, Institution of Engineers (India), and life member of Indian Society for Technical Education (ISTE), System Society of India (SSI) and Soft Computing Research Society (SCRS) of India. He also holds Chartered Engineer (India) certificate.